Precisely Composition Controlled Synthesis of $Cu_{0.5}Ni_{0.5}$ Alloy with Optimum Catalytic Activity

XU Xing-Liang(徐兴良);LI Li-Ping(李莉萍);ZHANG Dan(张丹);LUO Jia-Jun(罗家俊);LI Guang-She (李广社)

State Key Laboratory of Inorganic Synthesis and Preparative Chemistry, College of Chemistry, Jilin University, Changchun 130012, *China*

ABSTRACT Alloys based on non-noble metals could be the next generation of high-performance catalysts for many chemical reactions. However, precisely composition controlled synthesis of non-noble alloys remains a significant challenge. In this work, we report a simple synthesis of $Cu_{0.5}Ni_{0.5}$ alloys without any component segregation. Its success relies on the use of Cu–Ni oxalate precursors, which are chelated in the proximity by oxalate ligands. One of the attractive features for the oxalate routes of catalyst preparation is that no classical support material is needed. The actual component ratios of the obtained $Cu_{0.5}Ni_{0.5}$ alloy are consistent with the initial ratio. $Cu_{0.5}Ni_{0.5}$ alloy shows a higher catalytic activity than pure Cu and Ni catalysts in the reduction of *p*-nitrophenol (4-NP) to *p*-aminophenol (4-AP) by sodium borohydride ($NaBH_4$) in an aqueous solution, and the performance depends strongly on the strong interaction between Cu and Ni. The findings reported here are highly helpful to understand the relationship between the synergistic effects in alloys and their catalytic performance, and therefore could provide appropriate strategies to obtain desirable catalysts with improved activity in various catalytic applications.

Keywords: catalytic reduction; CuNi bimetallic alloy; *p*-nitrophenol; $NaBH_4$;
DOI: 10.14102/j.cnki.0254-5861.2011-1727

1 INTRODUCTION

Alloys have received considerable interest due to their potential applications in various chemical and physical processes, such as hydrogen storage, magnetic sensors, hydrogenation, fuel cell, ammonia decomposition, catalytic reforming, water gas shift reaction and so on[1-4]. Noble metal alloys have been generally utilized in catalytic reactions of various fields[5-8]. However, due to the high cost and limited supply of noble metals, the improvement of catalytic efficiency and the cost reduction are the top priorities.

Alternatively, alloys based on non-noble metals could be the next generation of high-performance catalysts for many chemical reactions.

Noble-metal free alloys are considered as promising catalysts with low cost, high activity and selectivity[9-11]. Owing to the synergistic effect of alloying between different metals, the activity and selectivity of alloys can be optimized by controlling the elemental composition. As a consequence, non-noble metal alloys (involving Cu, Fe, Co, and Ni) with different compositions have been synthesized by diverse methods[12]. Among all these alloys, CuNi alloys are promising candidates[12-14]. Nevertheless, the reduction potentials for the components of Cu and Ni metals are generally much lower than those of noble metals. As a result, more strenuous reaction conditions are required to prepare CuNi alloys[15-17]. For instance, toxic organic capping agents, solvents, reducing agents and organo-metals have been utilized to increase the reduction potentials. Besides, the differences in reduction potentials for Cu and Ni metals also limit the formation of alloys[18-20]. Therefore, it is necessary to develop simple and green methods to synthesize CuNi alloys with desired compositions.

Based on the above considerations, we report a simple synthesis of $Cu_{0.5}Ni_{0.5}$ alloy without any component segregation. Its success relies on the use of Cu–Ni oxalate precursors, which are chelated in the proximity by oxalate ligands[21-23]. Using this strategy, the actual component ratio of the obtained $Cu_{0.5}Ni_{0.5}$ alloy is consistent with the initial ratio. $Cu_{0.5}Ni_{0.5}$ alloy exhibits high activity in the reduction of *p*-nitrophenol (4-NP) by sodium borohydride ($NaBH_4$) in an aqueous solution.

2 EXPERIMENTAL

2. 1 Chemicals and materials

$Cu(NO_3)_2$ $3H_2O$ (> 98%), $Ni(NO_3)_2$ $6H_2O$ (> 98%), $H_2C_2O_4$ $2H_2O$ (> 99%), sodium borohydride ($NaBH_4$), and acetone were purchased from Shanghai Chemical Reagent company, and *p*-nitrophenol (4-NP) was purchased from Sigma-Aldrich Chemicals company. All chemical reagents were used as received without further purification**.**

2. 2 Synthesis of $Cu_{0.5}Ni_{0.5}$ alloys

$Cu_{0.5}Ni_{0.5}$ alloy was prepared by thermal decomposition of Cu–Ni oxalate precursors. In a typical synthesis of $Cu_{0.5}Ni_{0.5}$ alloy, an amount of oxalic acid (4 mmol) was dissolved in 20 mL acetone at room temperature. $Cu(NO_3)_2$ $3H_2O$ (0.5 mmol) and $Ni(NO_3)_2$ $6H_2O$ (0.5 mmol) were dissolved in 10 mL acetone

at room temperature. Then, the metal nitrate solution was added into the oxalic acid solution, and the mixed solution was stirred for 2 h. Finally, the obtained Cu−Ni oxalate precipitate was filtered, washed with acetone for several times, and dried overnight at 80 ℃.

Cu−Ni oxalate was calcined in a temperature-programmed manner (10% H_2 in Ar as vector gas at a volumetric flow rate of 30 mL min^{-1} using a ramp of 3 ℃ min^{-1} up to 450 ℃ for 3 h). The product thus obtained was passivated in a mixed atmosphere (1% O_2 and 99% Ar) at 25 ℃ for 30 min. Then, the alloy sample was obtained.

For comparison, pure Cu and Ni metals were also prepared, just adopting the similar procedure to that for alloy sample.

2. 3 Sample characterization

X-ray diffraction (XRD) patterns of the samples were recorded using D/MAX 2550 Advance X-ray diffractometer with Cu$K\alpha$ radiation source operated at 30 kV and 20 mA. Data were collected from 2θ between 40 ° and 80 ° with a step of 0.02 ° at a scanning speed of 5 °/min. FT-IR spectra of the sample were examined using by a Jasco FT/IR-410 in air at room temperature using 420 Herschel series in KBr dispersion. X-ray photoelectron spectroscopy (XPS) measurements were performed using ESCALAB250 photoelectron spectrometer equipped with a charge neutralizer and a Mg$K\alpha$ X-ray source. Thermogravimetry (TG: Perkin-Elmer) was carried out for the precursor powder in air from 25 to 800 °C at a constant heating rate for 10 °C min^{-1}. Morphologies of the as-synthesized samples were recorded using a field emission scanning electron microscope (FE-SEM) equipped with an EDX. Transmission electron microscopy (TEM) image was recorded on a JEOL 3010 with 300 kV acceleration voltages. UV-Vis absorption spectroscopy was carried out on a Shimadzu UV-3600 UV-Vis-NIR spectrophotometer in a wavelength range of 300～1000 nm.

2. 4 Catalytic activity test

10 mL of 4-NP aqueous solution (200 ppm) and 10 mL of freshly prepared aqueous $NaBH_4$ (0.06 M) were successively added into 20 mL of deionized water in a beaker. Next, 2 mg of catalyst was added into the mixture. The color of the solution changed gradually from yellow to transparent as the reaction proceeded. UV-vis spectrometry was used to monitor the change in absorbance at a time interval of 1 min.

3 RESULTS AND DISCUSSION

3. 1 Characterization of the obtained Cu−Ni oxalates

Cu−Ni oxalates were first prepared prior to the formation of CuNi alloy. The crystal structures of the obtained Cu−Ni oxalates were characterized by XRD. The fresh $Cu_{0.5}Ni_{0.5}$ oxalate was composed of copper oxalate hydrate and nickel oxalate hydrate phase, since the XRD peaks could be indexed to CuC_2O_4 xH_2O (JCPDS 21-0297) and orthorhombic phase NiC_2O_4 $2H_2O$ (JCPDS 25-0582), respectively[23]. From the data comparison between nickel oxalate (Fig. 1c) and $Cu_{0.5}Ni_{0.5}$ oxalate (Fig. 1b) with a higher nickel content, the peaks of $Cu_{0.5}Ni_{0.5}$ oxalate were seen characteristic of the nickel oxalate hydrate in an orthorhombic phase. The XRD peak at 2θ = 18.58^0 became more pronounced with the increase of Ni content, which could be ascribed to the diffraction of plane (202) of the nickel oxalate.

In order to further determine the coordination environment of Cu−Ni oxalates, FT-IR spectra of the oxalate samples were recorded (Fig. 2). It can be seen that all samples showed similar absorption spectrum. The strong band located at 3370 cm^{-1} is assigned to the stretching vibration of O–H group. The presence of carboxylate group in oxalate samples is confirmed by two bands at 1620 cm^{-1} for the asymmetric stretching vibrations and 1360 cm^{-1} for the symmetric stretching vibrations[24]. The band at 1317 cm^{-1} is assigned to the symmetric γ(C–O), which indicates the presence of bridging oxalates with all four oxygen atoms coordinated to the metal atoms[25, 26].

In this work, $Cu_{0.5}Ni_{0.5}$ alloy was synthesized by thermal decomposition of oxalates. In order to determine the suitable calcination temperature, all samples were studied by thermogravimetric (TG) analysis (Fig. 3). TG curves of Fig. 3 clearly showed that all oxalates underwent three stages. The first stage observed in the temperature range of 35～100 ℃ corresponds to the loss of adsorbed water. The second one begins at about 100 ºC and ends at about 250 ℃, which is attributed to the release of crystal water from MeC_2O_4 mH_2O to MeC_2O_4. The third one begins at about 250 ℃ and ends at about 450 ℃, showing a mass loss closer to the theoretical one for the decomposition of MeC_2O_4 to MexOy and Me with a release of CO_2 and CO gasses[27-29]. Based on the reduction temperature of oxalates in TG analysis, the calcination temperature was set at 450 ℃ for the subsequent alloying.

3. 2 Characterization of the obtained $Cu_{0.5}Ni_{0.5}$ alloy

The crystal structures of pure Cu and Ni metals and $Cu_{0.5}Ni_{0.5}$ alloy were monitored by XRD. Fig. 4 shows the standard diffraction data for metal Cu and Ni. The diffraction peaks of all samples are assigned to the (111), (200) and (220) planes, respectively, as confirmed by the standard data of fcc structure for $Cu_{0.5}Ni_{0.5}$ alloy[12, 30]. The diffraction peaks for alloy sample are distributed between those of pure copper and pure nickel, which confirms the formation of solid solution between Cu and Ni. Further, the content of Cu in

$Cu_{0.5}Ni_{0.5}$ alloy was estimated based on the Vegard's law that claims a linear relation between lattice parameter of an alloy and its composition. For most catalytic reactions, the surface area of catalyst is important because of its relevance to the absorption and desorption of reactants. BET data of the as-prepared sample are extremely low (<5 m^2/g), which could help one to eliminate the influence of contact area on the catalytic performance.

Fig. 5a shows SEM image of $Cu_{0.5}Ni_{0.5}$ alloy. SEM image clearly illustrates that the bimetallic particles are primarily spherical in nature, and the small particles were self-assembled to form bigger aggregates. TEM images further confirm that the obtained $Cu_{0.5}Ni_{0.5}$ alloy was spherical morphology. Fig. 5f shows a high-resolution TEM (HRTEM) image of $Cu_{0.5}Ni_{0.5}$ alloy. The interfringe distance of 0.205 nm is slightly smaller that of 0.208 nm for Cu (111) spacing, but larger than that of 0.203 nm for Ni (111) spacing. To analyze the structure and elemental composition of the alloys, SEM-energy dispersive X-ray (EDX) elemental mapping images of the $Cu_{0.5}Ni_{0.5}$ alloy are presented in Fig. 5 (c～e), which confirms the high dispersion of Cu and Ni in forming alloy structures without significant segregation of each component. As shown in Fig. 5b, the molar ratio of Cu to Ni is about 50:50, which agrees well with the initial ratio. This suggests that the metal precursors were reduced completely and transformed into $Cu_{0.5}Ni_{0.5}$ alloy. The above analyses further confirm the successful preparation of $Cu_{0.5}Ni_{0.5}$ alloy.

The chemical states of Cu and Ni in $Cu_{0.5}Ni_{0.5}$ alloy were further determined by XPS spectra. In the full spectrum of $Cu_{0.5}Ni_{0.5}$ alloy (Fig. 6a), the signals of C 1*s*, O 1*s*, Ni 2*p*, and Cu 2*p* can be clearly seen in the binding energy region from 0 to 1200 eV. XPS spectra of Cu 2*p* (Fig. 6b) exhibit two strong peaks at 932.3 and 952.5 eV, corresponding to Cu $2p_{3/2}$ and Cu $2p_{1/2}$, respectively. The binding energy value indicated the presence of metallic Cu^0[13, 31], whereas, the minor peaks located at 934.4 eV and low intensity satellites at 940～945 eV can be attributed to Cu^{2+}, as reported elsewhere[32-34]. Ni 2*p* spectra (Fig. 6c) also exhibited spin-orbital peaks. The photoelectron peak at 852.5 eV is assigned to Ni^0[30]. Besides this, the signal related to Ni^{2+} was also detected at a binding energy of 855.8 eV [30, 35, 36]. Therefore, Ni species was partially oxidized to form NiO. In addition to these peaks, a shake-up satellite peak in the region of 860～865 eV also confirms the existence of small amount of NiO[37]. The presence of copper and nickel oxides in the alloy suggests that a thin oxidized layer was formed, which is conducive to the stability of alloy.

3. 3 Application of $Cu_{0.5}Ni_{0.5}$ alloy for catalytic reduction of 4-NP

Reduction of 4-NP by $NaBH_4$ in aqueous solution is a model reaction[38, 39] that can be used for examining the catalytic activity of the as-prepared catalyst. For this purpose, the advantages of $Cu_{0.5}Ni_{0.5}$

alloy were explored to study the reduction of 4-NP to *p*-aminophenol (4-AP) in the presence of $NaBH_4$ at room temperature. As observed in Fig. 7a, 4-NP solution exhibited a strong absorption peak at 317 nm, which is remarkably red-shifted to 400 nm when treated with an aqueous solution of $NaBH_4$ only[40]. At the same time, the color of the solution changed from light to dark yellow. The absorption peak immediately shifted from 317 to 400 nm, probably because of the formation of *p*-nitrophenolate ions under alkaline condition with $NaBH_4$[41]. It should be noted that $NaBH_4$ is not able to reduce 4-NP without catalysts, even though it is considered as the electron donor and hydrogen source. The peak at 400 nm stayed unchanged for over 4 min in the absence of the catalyst (Fig. 7b), which demonstrates that the reduction reaction did not proceed without catalyst.

The catalytic activities of the as-prepared $Cu_{0.5}Ni_{0.5}$ alloy and the pure Cu and Ni metals were compared in the reaction of 4-NP reduction. Fig. 8 shows the time-dependent absorption of solution over the catalyst in the presence of excess $NaBH_4$. The maximum absorbance peak at 400 nm gradually declines as the reduction reaction time proceeds. Meanwhile, the color of the solution is also gradually dropped from dark yellow to colorlessness, accompanying with a concomitant increase of the peak at 300 nm, which indicates the reduction of 4-NP to 4-AP. The UV-visible absorption spectra showed an isosbestic point between two absorption peaks, suggesting that 4-NP compound was gradually converted to 4-AP without any side reaction. As indicated from UV-visible absorption spectra in Fig. 8a, it took 24 min for Cu to complete the catalytic reaction. For Ni (Fig. 8b), more than 40 min is needed for completing the catalytic reaction, which demonstrates that the catalytic activity of Ni was obviously lower. Comparatively, for $Cu_{0.5}Ni_{0.5}$ alloy (Fig. 8c), the complete reaction time dramatically decreased to 10 min, which showed a great enhancement of the catalytic activity. The reduction reaction completes at much shorter time for bimetallic alloy nanocrystals when compared to monometallic Cu and Ni.

To figure out the role of $Cu_{0.5}Ni_{0.5}$ alloy in this reduction conversion, the kinetic analysis of these reactions was carried out, as described from the temporal decay of these peaks. The ratio of C_t to C_0 (C_t and C_0 are 4-NP concentrations at time t and 0, respectively) was measured from the relative intensity of the respective absorbance A_t/A_0. As shown in Fig. 8d, without catalysts, the maximum absorption peak remains unchanged, indicating that the presence of $NaBH_4$ alone cannot initiate the conversion reaction even with a large excess amount. Alternatively, introducing pure Cu or Ni into the reaction system gives a moderate conversion, and thus pure Cu or Ni is active for the reduction of 4-NP. It is observed from Fig. 8d that the reduction reaction completes at much shorter time over the $Cu_{0.5}Ni_{0.5}$ alloy when compared to monometallic

Cu and Ni particles.

In order to study the activity of the catalyst, the pseudo-first-order reaction with regard to 4-NP concentration is used to evaluate the kinetic rate constant. The kinetic equation for the reduction can be written as,

$$\frac{dC_t}{dt} = kC_t \quad \text{or} \quad \ln\left(\frac{Ct}{C0}\right) = \ln\left(\frac{At}{A0}\right) = -kt \qquad (1)$$

where C_t is the concentration of 4-NP at time 't' and 'k' is the rate constant, which can be obtained from the decrease in the peak intensity at 400 nm with time. The catalytic performance of $Cu_{0.5}Ni_{0.5}$ alloy, the monometallic Cu and Ni particleswere obtained by calculating the rate constants from UV-Vis absorption spectra. The rate constants (k) of the reduction of 4-NP to 4-AP were estimated from diffusion-coupled first order reaction kinetics. The k value obtained for the reduction of 4-NP for $Cu_{0.5}Ni_{0.5}$ alloy is 0.31 min^{-1}, about twice higher than 0.15 min^{-1} for Cu and 0.12 min^{-1} for Ni. According to the rate constant, the catalytic activity of the $Cu_{0.5}Ni_{0.5}$ alloy for the reduction of 4-NP is higher than other noble metals reported in other literature[42, 43]. This could be the synergistic effect between Cu and Ni in alloys that plays a leading role in improving the catalytic properties. In the reduction of aromatic nitro-compounds, it is believed that *p*-nitrophenolate ions are adsorbed by the catalyst, and brohydride ions react with the catalyst and transfer a surface hydrogen species and electrons to them, thereby resulting in an efficient reduction of $-NO_2$ group[44]. The interaction between Cu and Ni here may facilitate the formation of the intermediate species and the transition of electrons.

Stability and reusability are of great importance for the practical applications of catalysts. The recyclability of catalytic reduction is carried out for $Cu_{0.5}Ni_{0.5}$ alloy for five successive cycles, as presented in Fig. 9. After five cycles, the catalytic activity retains high as 82%, showing a high stability for $Cu_{0.5}Ni_{0.5}$ alloy. The slight decreases in catalytic activity for the fourth and fifth cycles are probably due to the loss of catalyst during the separation and reuse of metal.

4 CONCLUSION

$Cu_{0.5}Ni_{0.5}$ alloy was prepared by thermal decomposition of Cu–Ni oxalates. The key was to the use of Cu–Ni oxalate precursors, and the metal precursors were reduced completely and transformed into alloys. The actual component ratios of the obtained $Cu_{0.5}Ni_{0.5}$ alloy are consistent with the initial ratios. In comparison with the monometallic Ni and Cu, $Cu_{0.5}Ni_{0.5}$ alloy exhibits an excellent catalytic activity and

selectivity for the reduction of *p*-nitrophenol by sodium borohydride in an aqueous solution, which might be related to the strong interaction between Cu and Ni. Therefore, CuNi alloys merited with low cost, simple preparation, and high activity, are uncovered to have a great potential in replacing noble metals for other catalytic applications.

REFERENCES

(1) Jiang, H. L.; Xu, Q. Recent progress in synergistic catalysis over heterometallic nanoparticles. *J. Mater. Chem.* **2011**, 21, 13705─13725.

(2) Kumar, M.; Soni, K.; Yadav, G. D. S.; Singh, S. D. Surfactant directed $Ag_{1-x}Ni_x$ alloy nanoparticle catalyzed synthesis of aromatic azo derivatives from aromatic amines. *Appl. Catal. A* **2016**, 525, 50─58.

(3) Mori, K.; Tanaka, H.; Dojo, M.; Yoshizawa, K.; Yamashita, H. Synergic catalysis of PdCu alloy nanoparticles within a macroreticular basic resin for hydrogen production from formic acid. *Chem. Eur. J.* **2015**, 21, 12085─12092.

(4) Güngörmez, K.; Metin, Ö. Composition-controlled catalysis of reduced graphene oxide supported CuPd alloy nanoparticles in the hydrolytic dehydrogenation of ammonia borane. *Appl. Catal. A* **2015**, 494, 22─28.

(5) Jiang, H. L.; Akita, T.; Ishida, T.; Haruta, M.; Xu, Q. Synergistic catalysis of Au@Ag core-shell nanoparticles stabilized on metal-organic framework. *J. Am. Chem. Soc.* **2011**, 133, 1304─1306.

(6) Gu, S.; Lu, Y.; Kaiser, J.; Albrecht, M.; Ballauff, M. Kinetic analysis of the reduction of 4-nitrophenol catalyzed by Au/Pd nanoalloys immobilized in spherical polyelectrolyte brushes. *Phys. Chem. Chem. Phys.* **2015**, 17, 28137─28143.

(7) Ye, W. C.; Yu, J.; Zhou, Y. X.; Gao, D. Q.; Wang, D. A.; Wang, C. M.; Xue, D. S. Green synthesis of Pt–Au dendrimer-like nanoparticles supported on polydopamine-functionalized graphene and their high performance toward 4-nitrophenol reduction. *Appl. Catal. B: Environ.* **2016**, 181, 371─378.

(8) Huang, X. M.; Wang, X. G.; Tan, M. W.; Zou, X. J.; Ding, W. Z.; Lu, X. G. Selective oxidation of alcohols on P123-stabilized Au–Ag alloy nanoparticles in aqueous solution with molecular oxygen. *Appl. Catal. A* **2013**, 467, 407─413.

(9) Singh, A. K.; Xu, Q. Synergistic catalysis over bimetallic alloy nanoparticles. *ChemCatChem.* **2013**, 5, 652─676.

(10) Aldosari, O. F.; Iqbal, S.; Miedziak, P. J.; Brett, G. L.; Jones, D. R.; Liu, X.; Edwards, J. K.; Morgan, D. J.; Knight, D. K.; Hutchings, G. J. Pd–Ru/TiO_2 catalyst – an active and selective catalyst for furfural hydrogenation. *Catal. Sci. Technol.* **2016**, 6, 234─242.

(11) Zhao, F. Z.; Gong, M.; Zhang, Y. H.; Li, J. L. The performance and structural study of CuNi alloy catalysts for methanol synthesis. *J. Porous Mater.* **2016**, 23, 733─740.

(12) Wang, M. L.; Wang, L. B.; Li, H. L.; Du, W. P.; Khan, M. U.; Zhao, S. T.; Ma, C.; Li, Z. Y.; Zeng, J. Ratio-controlled synthesis of CuNi octahedra and nanocubes with enhanced catalytic activity. *J. Am. Chem. Soc.* **2015**, 137, 14027─14030.

(13) Yen, H.; Seo, Y.; Kaliaguine, S.; Kleitz, F. Role of metal-support interactions, particle size, and metal-metal synergy in CuNi nanocatalysts for H_2 generation. *ACS Catal.* **2015**, 5, 5505─5511.

(14) Simonsen, S. B.; Chakraborty, D.; Chorkendorff, I.; Dahl, S. Alloyed Ni-Fe nanoparticles as catalysts for NH_3 decomposition. *Appl. Catal. A* **2012**, 447, 22─31.

(15) Yang, J. L.; Shen, X. P.; Ji, Z. Y. Zhou, H.; Zhu, G. X.; Chen, K. M. *In situ* growth of hollow CuNi alloy nanoparticles on reduced graphene oxide nanosheets and their magnetic and catalytic properties. *Appl. Surf. Sci.* **2014**, 316, 575─581.

(16) Biswas, M.; Saha, A.; Dule, M.; Manda, T. K. Polymer-assisted chain-like organization of CuNi alloy nanoparticles: solvent-adoptable pseudohomogeneous catalysts for alkyne-azide click reactions with magnetic recyclability. *J. Phys. Chem. C* **2014**, 118, 22156─22165.

(17) Guo, H. Z.; Chen, Y. Z.; Ping, H. M.; Wang, L. S.; Peng, D. L. One-pot synthesis of hexagonal and triangular nickel-copper alloy nanoplates and their magnetic and catalytic properties. *J. Mater. Chem.* **2012**, 22, 8336─8344.

(18) Arbeláez, O.; Reina, T. R.; Ivanova, S.; Bustamante, F.; Villa, A. L.; Centeno, M. A.; Odriozola, J. A. Mono- and bimetallic Cu-Ni structured catalysts for the water gas shift reaction. *Appl. Catal. A* **2015**, 497, 1─9.

(19) Feng, J.; Zhang, C. P. Preparation of Cu–Ni alloy nanocrystallites in water-in-oil microemulsions. *J. Colloid. Interf. Sci.* **2006**, 293, 414─420.

(20) Bonet, F.; Grugeon, S.; Dupont, L.; Urbina, R. H.; Guery, C. J.; Marascona, T. Synthesis and characterization of bimetallic Ni–Cu particles. *J. Solid State Chem.* **2003**, 172, 111─115.

(21) Xiang, Y. Z.; Barbosa, R.; Kruse, N. Higher alcohols through CO hydrogenation over CoCu catalysts: influence of precursor activation. *ACS Catal.* **2014**, 4, 2792─2800.

(22) Xiang, Y. Z.; Chitry, V.; Liddicoat, P.; Felfer, P.; Cairney, J.; Ringer, S.; Kruse, N. Long-chain terminal alcohols through catalytic CO hydrogenation. *J. Am. Chem. Soc.* **2013**, 135, 7114─7117.

(23) Wang, H. Y.; Lua, A. C. Methane decomposition using Ni–Cu alloy nano-particle catalysts and catalyst deactivation studies. *Chem. Eng. J.* **2015**, 262, 1077─1089.

(24) Niasari, M. S.; Mir, N.; Davar, F. Synthesis and characterization of Co_3O_4 nanorods by thermal decomposition of cobalt oxalate. *J. Phys. Chem. Solids* **2009**, 70, 847─852.

(25) Hamed, M. N.; Kama, H. R. The effect of particle size on the kinetics of thermal decomposition of $Co(C_2O_4)$ $2H_2O$ nanopowders under non-isothermal conditions. *J. Therm. Anal. Calorim.* **2016**, 123, 675─686.

(26) Nasrabadi, M. R.; Pourmortazavi, S. M.; Dehaghani, A. A. D.; Hajimirsadeghi, S. S.; Zahedi, M. M. Synthesis and characterization of copper oxalate and copper oxide nanoparticles by statistically optimized controlled precipitation and calcination of precursor. *CrystEngComm.* **2013**, 15, 4077─4086.

(27) Yang, M. Q.; He, J. H.; Hu, X. H.; Yan, C. X.; Cheng, Z. X. Synthesis of nanostructured copper oxide via oxalate precursors and their sensing properties for hydrogen cyanide gas. *Analyst.* **2013**, 138, 1758–1763.

(28) Sarada, K.; Muraleedharan, K. Effect of addition of silver on the thermal decomposition kinetics of copper oxalate. *J. Therm. Anal. Calorim.* **2016**, 123, 643–651.

(29) Kwaka, B. S.; Leea, G.; Parkb, S. M.; Kang, M. Effect of MnO_x in the catalytic stabilization of Co_2MnO_4 spinel during the ethanol steam reforming reaction. *Appl. Catal. A* **2015**,503, 165─175.

(30) Fang, H.; Wen, M.; Chen, H. X.; Wu, Q. S.; Li, W. Y. Graphene stabilized ultra-small CuNi nanocomposite with high activity and recyclability toward catalyzing the reduction of aromatic nitro-compounds. *Nanoscale* **2016**, 8, 536–542.

(31) Wang, Y.; Sang, S. Y.; Zhu, W.; Gao, L. J.; Xiao, G. M. CuNi@C catalysts with high activity derived from metal-organic frameworks precursor for conversion of furfural to cyclopentanone. *Chem. Eng. J.* **2016**, 299,104–111.

(32) Kaya, M.; Zahmakiran, M.; Özkar, S.; Volkan, M. Copper(0) nanoparticles supported on silica-coated cobalt ferrite magnetic particles: cost effective catalyst in the hydrolysis of ammonia-borane with an exceptional reusability performance. *ACS Appl. Mater. Interfaces* **2012**, 4, 3866─3873.

(33) Yamada, Y.; Yano, K.; Fukuzumi, S. Catalytic application of shape-controlled Cu_2O particles protected by Co_3O_4 nanoparticles for hydrogen evolution from ammonia borane. *Energy Environ. Sci.* **2012**, 5, 5356─5363.

(34) Xie, R. F.; Fan, G. L.; Yang, L.; Li, F. Hierarchical flower-like Co–Cu mixed metal oxide microspheres as highly efficient catalysts for selective oxidation of ethylbenzene. *Chem. Eng. J.* **2016**, 288, 169─178.

(35) Lin, J.; Guliants, V. V. Hydrogen production through water-gas shift reaction over supported Cu, Ni, and Cu[BOND]Ni nanoparticle catalysts prepared from metal colloids. *ChemCatChem.* **2012**, 4, 1611─1621.

(36) Kang, J.; Han, R. R.; Wang, J.; Yang, L.; Fan, G. L.; Li, F. *In situ* synthesis of nickel carbide-promoted nickel/carbon nanofibers nanocomposite catalysts for catalytic applications. *Chem. Eng. J.* **2015**, 275, 36─44.

(37) Prieto, P.; Nisto, V.; Nouneh, K.; Oyama, M.; Lefdil, M. A.; D áz, R. XPS study of silver, nickel and bimetallic silver-nickel nanoparticles prepared by seed-mediated growth. *Appl. Surf. Sci.* **2012**, 258, 8807─8813.

(38) Chinnappan, A.; Tamboli, A. H.; Chung, W. J.; Kim, H. Green synthesis, characterization and catalytic efficiency of hypercross-linked porous polymeric ionic liquid networks towards 4-nitrophenol reduction. *Chem. Eng. J.* **2016**, 285, 554–561.

(39) Huang, C. J.; Ye, W. Q.; Liu, Q. W.; Qiu, X. Q. Dispersed Cu_2O octahedrons on h‐ BN nanosheets for p‐ Nitrophenol reduction. *ACS Appl. Mater. Interfaces* **2014**, 6, 14469─14476.

(40) Lin, Y. Y.; Qiao, Y.; Wang, Y. J.; Yan, Y.; Huan, J. B. Self-assembled laminated nanoribbon-directed synthesis of noble metallic nanoparticle -decorated silica nanotubes and their catalytic applications. *J. Mater. Chem.* **2012**, 22, 18314–18320.

(41) Layek, K.; Kantam, M. L.; Shirai, M.; Hamane, D. N.; Sasaki, T.; Maheswaran, H. Gold nanoparticles stabilized on nanocrystalline magnesium oxide as an active catalyst for reduction of nitroarenes in aqueous medium at room temperature. *Green Chem.* **2012**, 14, 3164─3174.

(42) Mondal, S.; Rana, U.; Bhattacharjee, R. R.; Malik, S. One pot green synthesis of polyaniline coated gold nanorods and its applications. *RSC Adv.* **2014**, 4, 57282─57289.

(43) Praharaj, S.; Nath, S.; Ghosh, S.; Kundu, S.; Pal, T. Immobilization and recovery of Au nanoparticles from anion exchange resin: resin-bound nanoparticle matrix as a catalyst for the reduction of 4-nitrophenol. *Langmuir.* **2004**, 20, 9889─9892.

(44) Herv és, P.; Lorenzo, M. P.; Marz án, L. M. L.; Dzubiella, J.; Lu, Y.; Ballauff, M. Catalysis by metallic nanoparticles in aqueous solution: model reactions. *Chem. Soc. Rev.* **2012**, 41, 5577─5587.

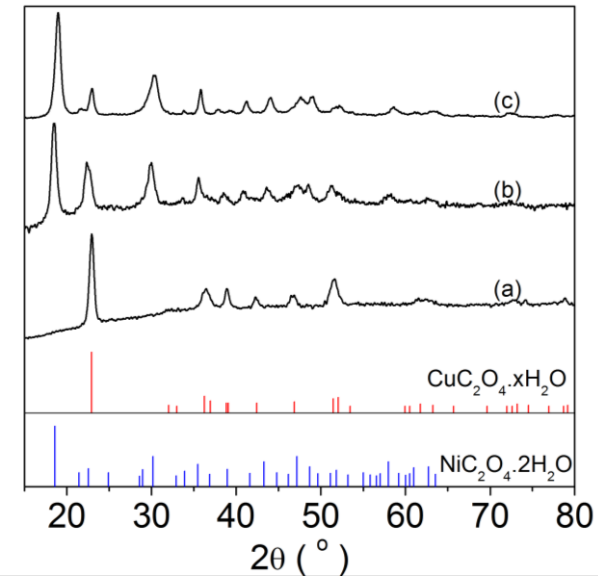

Fig. 1. X-ray diffraction patterns of oxalate precursors: (a) cupric oxalate, (b) $Cu_{0.5}Ni_{0.5}$ oxalate, and (c) nickel oxalate

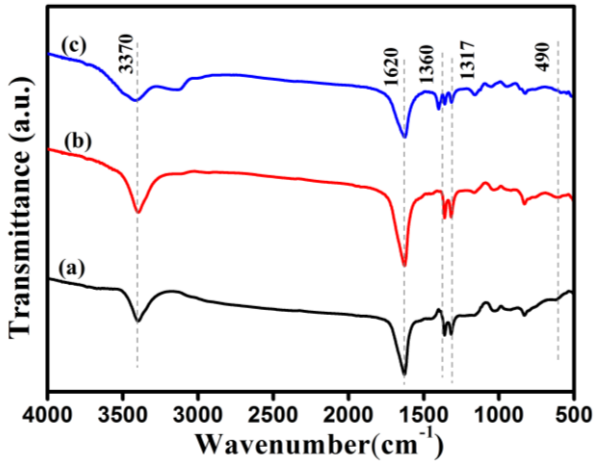

Fig. 2. FT-IR spectra of oxalate precursors: (a) cupric oxalate, (b) $Cu_{0.5}Ni_{0.5}$ oxalate, and (c) nickel oxalate

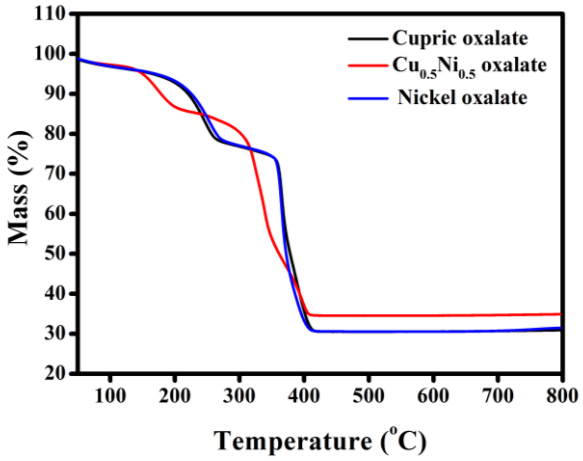

Fig. 3. TG curves of the given oxalate precursors

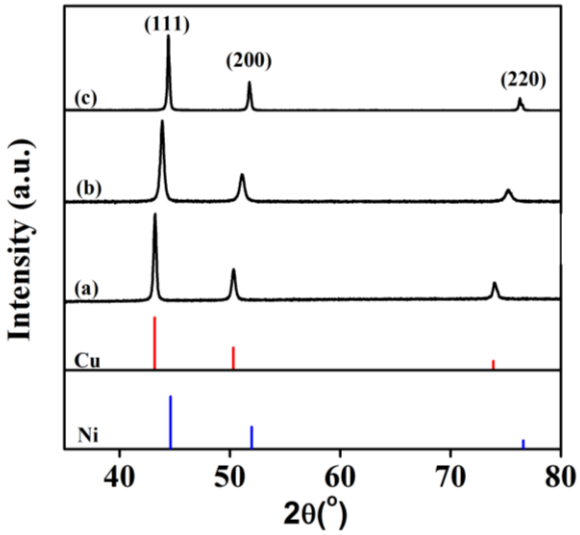

Fig. 4. XRD patterns of (a) Cu, (b) $Cu_{0.5}Ni_{0.5}$ alloy and (c) Ni

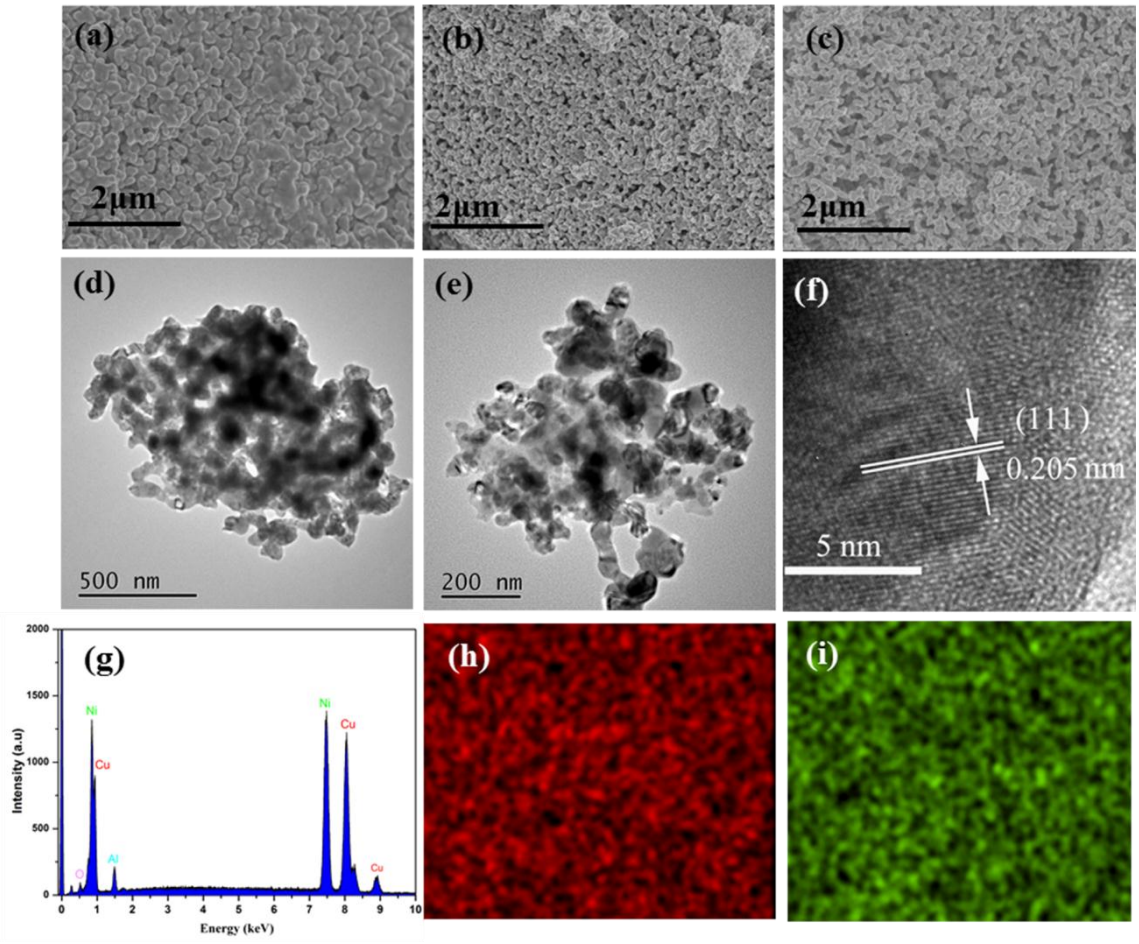

Fig. 5. SEM images of (a) Cu, (b) Ni, and (c) $Cu_{0.5}Ni_{0.5}$ alloy, (d-e) TEM image of $Cu_{0.5}Ni_{0.5}$ alloy, and (f) HTEM images of $Cu_{0.5}Ni_{0.5}$ alloy, (g) SEM-EDS spectrum, SEM-EDS elemental mapping images of (h) Cu and (i) for $Cu_{0.5}Ni_{0.5}$

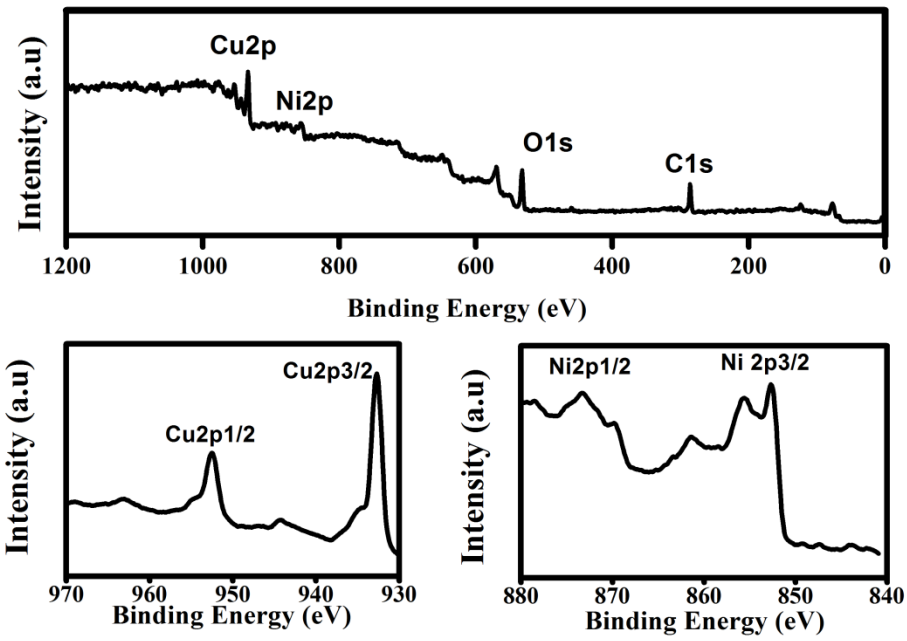

alloy

Fig. 6. XPS analysis of $Cu_{0.5}Ni_{0.5}$ alloy: (a) Full spectrum in the binding energy region from 0 to 1200 eV; detailed spectrum of (b) Cu 2*p* and (c) Ni 2*p*

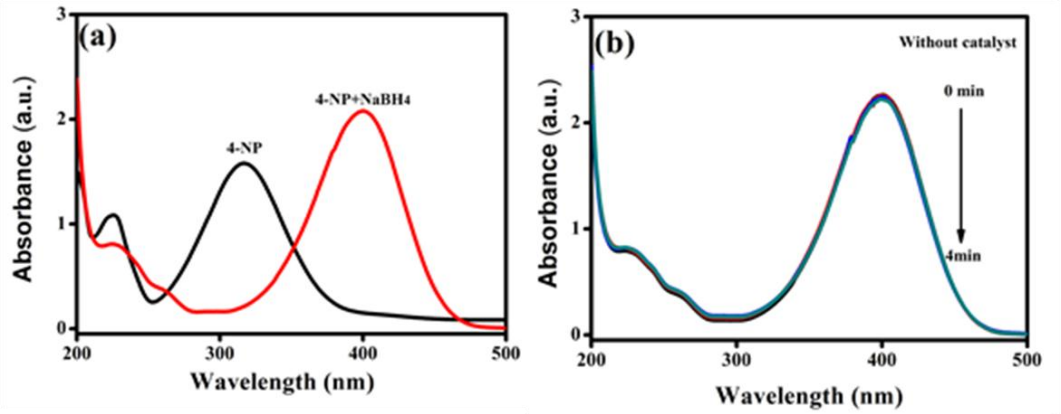

Fig. 7. (a) UV-visible absorption spectra of 4-NP with and without $NaBH_4$, and (b) time-dependent UV-visible absorption spectra for the reduction of 4-NP with $NaBH_4$ in the absence of catalyst

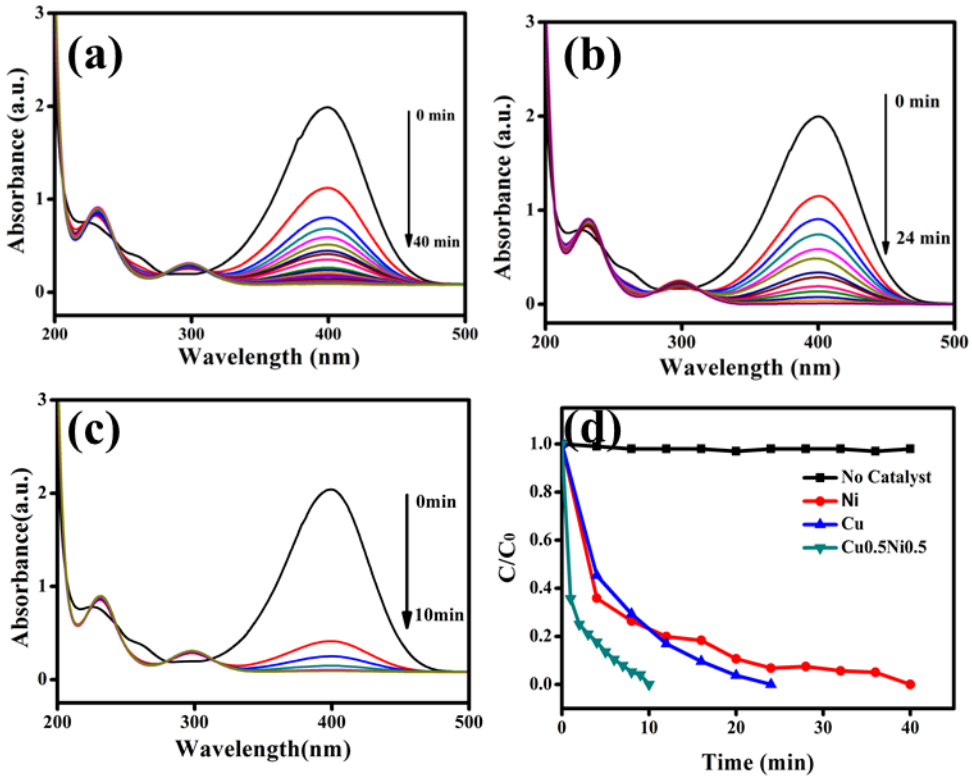

Fig. 8. Evolution of UV-vis spectra of 4-NP solution with various catalysts: (a) Cu, (b) Ni, (c) $Cu_{0.5}Ni_{0.5}$; (d) the variation of relative intensity of 4-NP with the reaction time in the presence of excess $NaBH_4$ over various catalysts. Square dots are the data without adding any catalyst

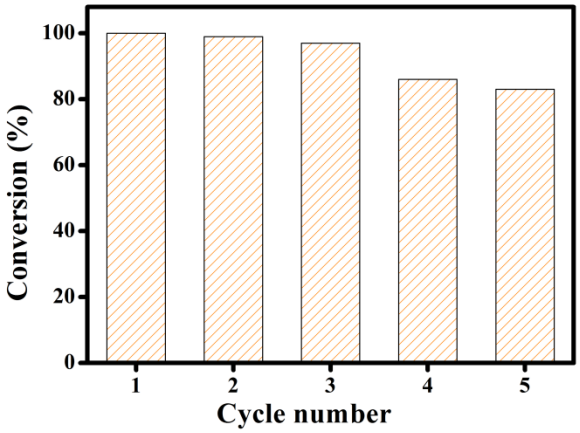

Fig. 9. Conversion of 4-NP for five successive cycles of reduction with the $Cu_{0.5}Ni_{0.5}$ alloy

Precisely Composition Controlled Synthesis of $Cu_{0.5}Ni_{0.5}$ Alloy with Optimum Catalytic Activity

XU Xing-Liang(徐兴良)　LI Li-Ping(李莉萍)　ZHANG Dan(张丹)

LUO Jia-Jun(罗家俊)　LI Guang-She(李广社)

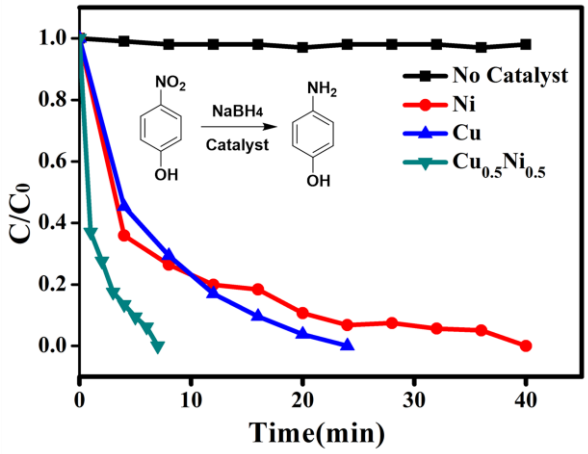

$Cu_{0.5}Ni_{0.5}$ alloy was prepared by thermal decomposition of Cu–Ni oxalates, which exhibits an excellent catalytic activity for the reduction of *p*-nitrophenol in comparison with monometallic Ni or Cu.